Two-Photon Imaging of Blood Flow in the Rat Cortex

Jonathan D. Driscoll, Andy Y. Shih, Patrick J. Drew, Gert Cauwenberghs and David Kleinfeld

Cold Spring Harb Protoc; doi: 10.1101/pdb.prot076513

Protocol

Two-Photon Imaging of Blood Flow in the Rat Cortex

Jonathan D. Driscoll, Andy Y. Shih, Patrick J. Drew, Gert Cauwenberghs, and David Kleinfeld

Cerebral blood flow plays a central role in maintaining homeostasis in the brain, and its dysfunction leads to pathological conditions such as stroke. Moreover, understanding the dynamics of blood flow is central to the interpretation of data from imaging modalities—such as intrinsic optical signaling and functional magnetic resonance imaging—that rely on changes in cerebral blood flow and oxygen level to infer changes in the underlying neural activity. Recent advances in imaging techniques have allowed detailed studies of blood flow in vivo at high spatial and temporal resolutions. We discuss techniques to accurately measure cerebral blood flow at the level of individual blood vessels using two-photon laser-scanning microscopy. By directing the scanning laser along a user-defined path, it is possible to measure red blood cell (RBC) velocity and vessel diameter across multiple vessels simultaneously. The combination of these measurements permits accurate assessment of total flux with sufficient time resolution to measure fast modulations in flux, such as those caused by heartbeat, as well as slower signals caused by vasomotion and hemodynamic responses to stimulus. Here, we discuss general techniques for animal preparation and measurement of blood flow with two-photon microscopy. We incorporate extensions to existing methods to accurately acquire flux data simultaneously across multiple vessels in a single trial. Central to these measurements is the ability to generate scan paths that smoothly connect user-defined lines of interest while maintaining high accuracy of the scan path.

MATERIALS

It is essential that you consult the appropriate Material Safety Data Sheets and your institution's Environmental Health and Safety Office for proper handling of equipment and hazardous material used in this protocol.

RECIPES: Please see the end of this article for recipes indicated by <R>. Additional recipes can be found online at http://cshprotocols.cshlp.org/site/recipes.

Reagents

Agarose (low melting point) (Type III-A from Sigma-Aldrich)
Dextrose (5% [w/v] in saline)
Fluorescent dye (e.g., fluoroscein-dextran [2 MDa; Sigma-Aldrich] or Texas Red-dextran [70 kDa; Invitrogen])

Prepare a 5% (w/v) solution in saline and freeze in aliquots at −20°C for later use.

Heparin (20 U/mL in saline) (for blood collection)
Isoflurane (anesthetic used for survival studies)
Lidocaine solution (2% [v/v])
Modified artificial cerebrospinal fluid (mACSF) (free of carbonate and phosphate) <R>
Ophthalmic ointment

Adapted from *Imaging in Neuroscience* (ed. Helmchen and Konnerth). CSHL Press, Cold Spring Harbor, NY, USA, 2011.

Cite this article as *Cold Spring Harb Protoc*; 2013; doi:10.1101/pdb.prot076513

Rose Bengal (1% [w/v] in saline; filtered before use)

Freeze the 1% Rose Bengal solution in aliquots at −20°C for later use. Rose Bengal is a photosensitizer used to induce clot formation in stroke models.

SurgiFoam (Edgepark)
Urethane or α-cholarlose (anesthetics used for terminal studies)
VetBond (3M)

Equipment

Blood gas monitor (RapidLab 248 from Bayer)
Blood pressure monitor (BP1 from World Precision Instruments for intra-arterial; XBP1000 from Kent Scientific for tail cuff measurements)
Catheter (Surflo from Terumo)
Cover glass (no. 1 thickness)
Dental acrylic (Grip Cement from Dentsply)
Dental drill (air-powered) (Silentaire)
Drill burrs (0.5- and 0.25-mm tip sizes) (Henry Schein)
Forceps (extra-sharp; Dumont no. 55) (Fine Science Tools)
Glass cutter
Head-frame (custom-made; see Fig. 1A)
Heat pad (feedback-regulated) (Harvard for rats; FHC for mice)
Hemostats
Isoflurane vaporizer (IsoTec)
Kimwipes
Optical breadboard with head holder (Fig. 1B) and devices for physiological support and monitoring
PE50 tubing (for femoral artery/vein catheters) (Intramedic)
Periosteal elevator (Roboz)
Pulse oximeter (Nonin for rats; Starr Life Sciences for mice)
Scalpel blades
Screwdriver (miniature)
Screws (self-tapping) (Small Parts Inc. 000-3/32)
Stereotaxic frame (Kopf)
Syringe needle (26-gauge)
Two-photon laser-scanning microscope (TPLSM)

Our TPLSM is a custom-design optimized for in vivo studies (Nguyen et al. 2006, 2009; Tsai and Kleinfeld 2009).

METHOD

Anesthesia

1. Anesthetize the rat.

   Common anesthetic choices include (i) urethane delivered intraperitoneally, that is, 1000 mg/kg body weight initial dose with 100 mg/kg supplements as required (Kleinfeld and Denk 2000) or (ii) initial isoflurane for surgery followed by a transition to intravenous delivery of α-chloralose for imaging, that is, an initial bolus at 50 mg/kg body weight for induction and continuous delivery of 40 mg/kg for maintenance (Devor et al. 2007). Both urethane and α-chloralose should be prepared fresh on the day of the experiment. Heating to ~60°C and agitation is necessary to dissolve α-chloralose. Neither urethane nor α-chloralose is suitable for survival experiments.

2. Check for lack of toe pinch reflex to ensure an adequate level of anesthesia.
3. Secure the rat in a stereotaxic frame.
4. Apply ophthalmic ointment to the eyes to keep them moist.

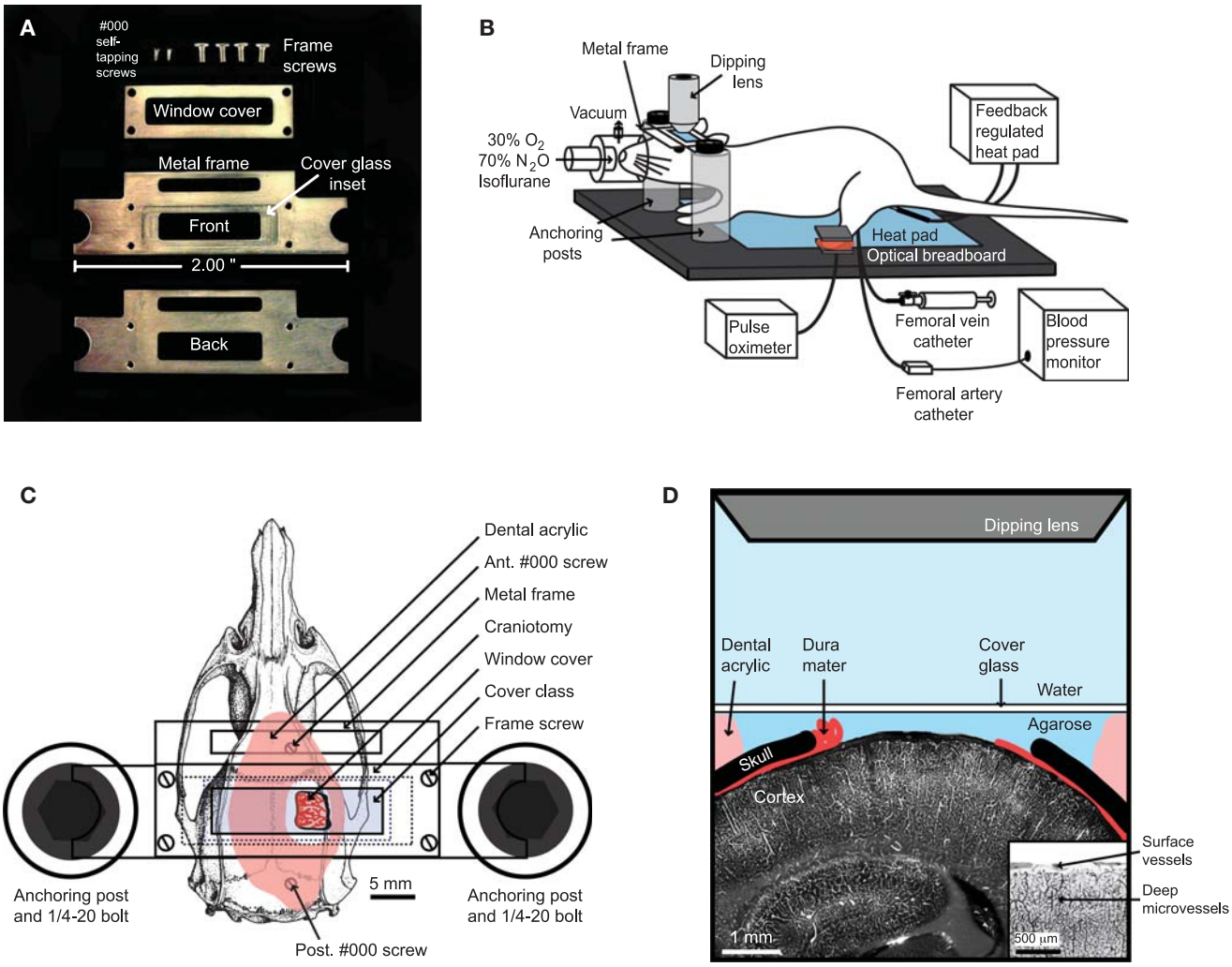

FIGURE 1. Setup for in vivo imaging of blood flow through a cranial window. (*A*) To immobilize the head of the animal during imaging, we designed a metal frame that could be cemented to the skull, and then anchored to an optical setup. The frame is constructed of type 410 stainless steel with dimensions of 2.00 inches long, 0.61 inches wide, and 0.029 inches thick, and can be secured between two posts in a standard optical breadboard. An inset region, 0.015 inches deep, borders the frame window to hold a cover glass over the craniotomy. The window cover, 0.015 inches thick of type 301 stainless steel, is then secured to the frame with four screws, sandwiching a no. 1 cover glass in place. (*B*) A typical experimental setup. Note: The metal frame attached to the skull is immobilized between two anchoring posts inserted into an optical breadboard. (*C*) Diagram of cranial window preparation for rat. (*D*) A cross-sectional view of the cranial window. (*Inset*) An inverted coronal view of surface vessels and deep microvessels that are targeted for occlusion.

5. Inject 0.1 mL of 2% (v/v) lidocaine subcutaneously into the scalp as a local anesthetic before incision (see Step 11).

Monitoring Requirements

The following procedures need to be performed throughout the surgery and during imaging.

6. Monitor heart and breathing rates with a pulse oximeter. They should remain within a normal range: 300–400 beats/min and 60–120 events/min.
7. Maintain body temperature at 37°C using a feedback-regulated rectal probe and heat pad.
8. Inject 5% (w/v) dextrose in saline intraperitoneally at 3 mL/kg body weight every 2 h to maintain body fluids and energy requirements.

9. Install a femoral artery catheter to collect blood samples and a femoral vein catheter to administer drugs (e.g., fluoroscein-dextran, Texas Red-dextran, or Rose Bengal). Monitor blood gases every 2 h.
10. Monitor arterial blood pressure continuously from the femoral arterial line. Alternatively, use the tail cuff method to noninvasively measure blood pressure at intermittent time points.

Cranial Window Surgery

Perform a craniotomy above the cortical area of interest (Kleinfeld et al. 1998; Mostany and Portera-Caillau 2008). (In our example application [see Discussion], this corresponds to the somatosensory area of parietal cortex in rat.) A custom-made head frame is cemented to the skull to provide a means to secure the animal under the microscope (Fig. 1). As a means to protect the brain and prevent motion artifacts, the exposed region of cortex is covered with agarose prepared in an artificial cerebrospinal fluid and sealed with a microscope coverslip. Note that an alternative technique for mice makes use of a thinned and reinforced skull to avoid exposing the brain at the price of restricted optical access (Drew et al. 2010b). All procedures must be performed in accordance with the relevant animal care guidelines.

11. Shave the surgical area and make a 4–5-cm incision down the midline of the scalp. Use a periosteal elevator to remove the thin periosteum from the surface of the skull.
12. Demarcate the location of the cranial window.

    We typically consider measurements over primary somatosensory cortex, which is the part of parietal cortex that nominally lies between −1 and −5 mm relative to the Bregma point and between 1 and 7 mm from the midline on the mediolateral axis for rats (Paxinos and Watson 1986).

13. Attach a custom metal frame to the skull with dental acrylic. The frame holds the head of the animal rigidly to the optical apparatus (Figs. 1A,B).
    i. Clean the soft tissue from the contact regions of the bone.
    ii. Apply a thin layer of VetBond.
    iii. Introduce small self-tapping screws into the anterior and posterior aspects of the skull. (Note that one of the screws passes through an opening in the frame.) Mechanically link the screws to the frame with dental cement (Fig. 1C).
    iv. Secure the threads of the screws to the bone with a small dab of VetBond.

        Note that the temporalis muscle may need to be retracted in some cases, and the temporal ridge may need to be flattened with a dental drill. This is to ensure that the metal head frame is cemented tangential to the cortical surface when imaging the lateral aspects of the barrel cortex.

14. Perform a craniotomy above the brain region of interest using a high-speed drill.
    i. Thin the skull throughout the entire window to approximately one-quarter of its original thickness using a 0.5-mm drill burr until the underlying pial vasculature becomes visible following application of mACSF. During drilling, flush the window regularly with mACSF to reduce heat buildup and to remove blood and bone shavings.
    ii. Carefully thin the edges of the window with a 0.25-mm burr until the bone begins to craze.
    iii. Use forceps to gently separate the bone flap from the skull without protruding too deeply.
    iv. Use two forceps to grasp adjacent corners of the loosened bone flap, and slowly peel it away from the underlying dura mater.
15. Reflect the dura to the edges of the window (Fig. 1D).
    i. Make a small incision using the cutting edge of a 26-gauge syringe needle. Bend the needle to an obtuse angle with hemostats to ensure that the cutting edge approaches the dura at a suitable angle.
    ii. Use two sharp no. 55 forceps to gently lift the dura away from the cortical surface, starting at the incision site, and tearing in small increments. Whenever possible, tear around large dural vessels to avoid bleeding.

Limit any dural bleeding with small pieces of Surgifoam soaked in mACSF, and Kimwipes twisted to a fine point with the fingers. Keep the cranial window moist with a piece of moist Surgifoam.

iii. Retract the dural flaps to the side of the window, and flush the cortical surface with mACSF.

It is crucial to avoid any damage to pial vessels. Hemorrhaging will alter cerebral blood flow, accelerate edema, and severely degrade imaging quality.

16. Fill the interior of the chamber with 1.5% (w/v) low-melting-point agarose dissolved in mACSF (Fig. 1D) (Kleinfeld and Delaney 1996). Dissolve the agarose by heating it in a microwave. The temperature of the agarose must not exceed 37°C when it is applied to the brain.
17. Immediately seal the chamber using a cover glass as a window (Fig. 1D). Resealing the craniotomy is crucial to protect the cortex and suppress motion from cranial pressure fluctuations caused by heartbeat and breathing. One edge of the window can remain uncovered to allow insertion of electrodes or micropipettes.
18. Suture the skin together around the frame, and trail agarose around the cover glass to hold water for the dipping lens.
19. Stabilize the animal on an optical breadboard for imaging, using the frame as a head support.

Our separate plate can be transported between surgical and imaging suites with the animal and all physiological monitoring devices assembled as one unit (Fig. 1B).

DISCUSSION

Example Application

An application of this technique is illustrated in Figure 2. A cranial window was generated over the rat somatosensory cortex. Intrinsic optical imaging was used to determine the locations of the hindlimb and forelimb cortical representation (Drew and Feldman 2009). The cerebral vasculature of the hindlimb somatosensory region was mapped using a TPLSM image stack obtained with a low magnification 4× objective (Fig. 2A). A single penetrating arteriole and neighboring ascending venule were selected for measurement under a 40× objective (Fig. 2B).

A scan path was created to traverse along the length of the lumen center, and across the lumen width for each vessel. The accuracy of the scan path can be verified by comparing the value of the mirror position encoder with the control voltage. Scan accuracy in user-selected linear scan paths is ~1 μm, whereas intervening segments that connect the user-defined regions and are not used in data analysis have a higher error, up to ~5 μm (Fig. 2C). The resulting line scan is a space–time image (Fig. 2D).

Portions of the scan path along the vessel length appear as streaks within the line-scan image. These streaks represent nonfluorescent RBCs that move through a fluorescent background. The *x*-axis represents the distance traveled by the RBCs, and the *y*-axis is the time. The centerline velocity is then calculated from the slope of the RBC streaks (Fig. 2E, right panel). Previously, singular value decomposition was used to find the slope of these streaks and calculate the RBC velocity (Kleinfeld et al. 1998; Schaffer et al. 2006). A faster method that can calculate the velocity in near real time makes use of the Radon transform (Drew et al. 2010a). In either case, the velocity is taken using windowed portions of the line scans, typically 25 msec of data for a Nyquist frequency of 20 Hz. This is sufficient to capture the fastest biological signal, the heart rate, without aliasing the second harmonic of the rate.

Portions of the scan path across the vessel width capture the diameter of the vascular lumen, because the fluorescently labeled blood plasma provides high contrast with the unlabeled region immediately outside the vessel. To increase the signal-to-noise ratio, multiple scans across the vessel diameter are averaged together before the profile is calculated. As with the velocity calculation, the diameter transform is made on a windowed portion of the data. Typically, the same window size as for velocity is used so that both parameters can be calculated on the same timescale.

Vessel diameter is calculated as full-width at half-maximum (FWHM) of the vessel profile (Fig. 2E, left). Because the intensity profile tends to decrease in the center of the vessel, where a large volume of

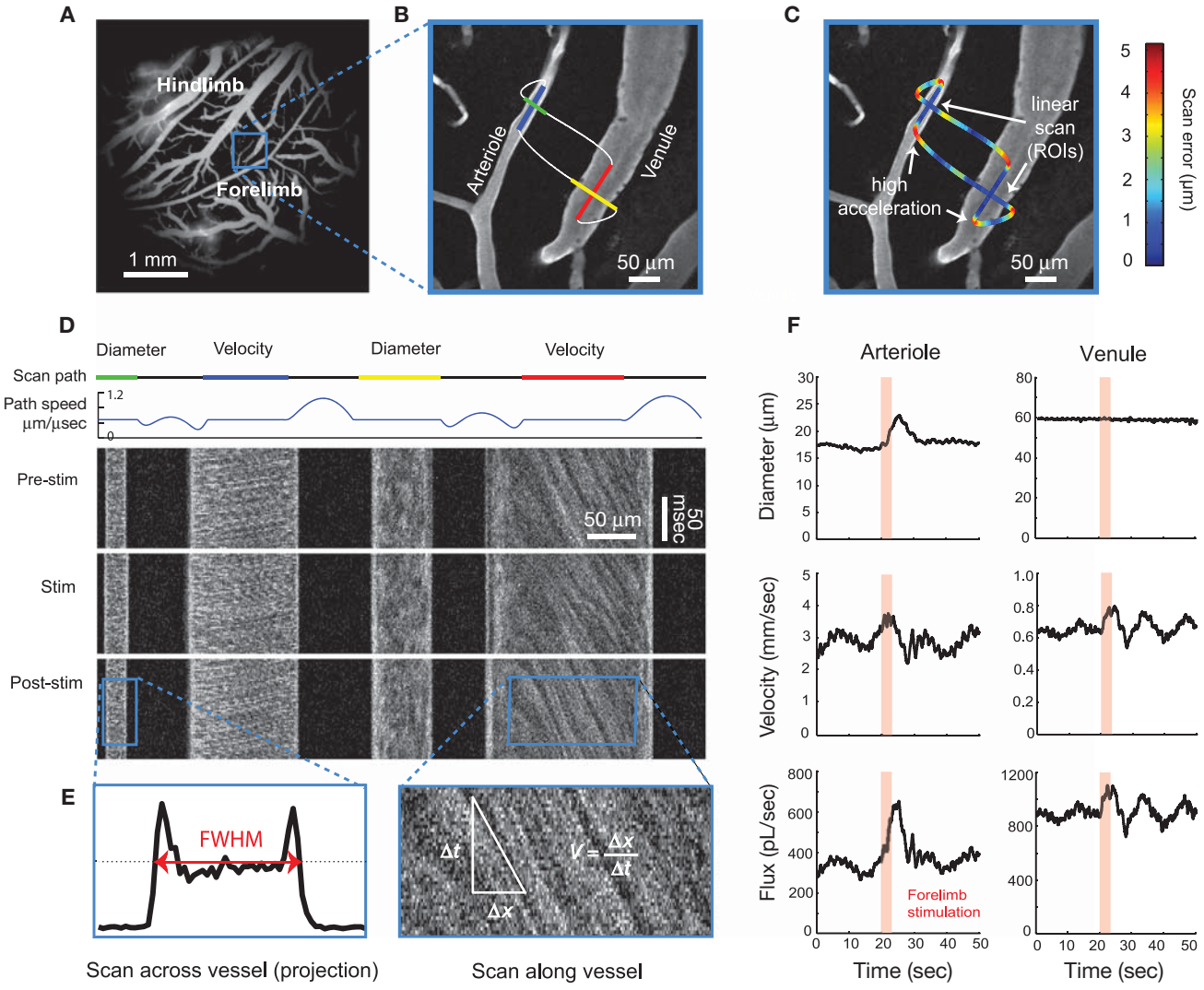

FIGURE 2. Simultaneous measurement of diameter and velocity in multiple vessels using spatially optimized line scans. (*A*) Image of fluorescently stained vessels in the somatosensory cortex of a Sprague Dawley rat. The forelimb and hindlimb representations across the cortex were mapped using intrinsic optical imaging. (*B*) Image of a surface arteriole and venule, with scan pattern superimposed. Portions of the scan path along the length are used to calculate RBC velocity, while portions across the diameter of the vessels are used to calculate diameter. Scans were acquired at a rate of 735 lines per second. (*C*) Scan path, colored to show the error between the desired scan path and the actual path the mirrors traversed. The error along linear portions of the image is ~1 µm, and increases when the mirrors undergo rapid acceleration. The error between successive scans of the same path is <0.15 µm, several times lower than the point-spread function of a TPLSM. (*D*) Mirror speed as a function of time. Note that portions used to acquire diameter and velocity data are constant speed (*top*). The line scans generated from the path can be stacked sequentially as a function of time to produce a raw cascade image (*bottom*). (*E*) Vessel diameter is calculated as the full width at half-maximum of a time average of several scans across the width of a vessel (*left*). RBC velocity calculated from the angle of the RBC streaks. (*F*) Data traces of diameter, velocity, and flux for the arteriole and venule, processed to remove heart rate and smoothed with a running window. Both vessels show an increase in flux in response to forelimb stimulation. In the arteriole, this flux increase is caused by simultaneous increase of lumen diameter and RBC velocity. In contrast, flux increase in the venule is due only to an increase in RBC velocity, as diameter is unchanged by stimulation.

RBCs exclude the fluorescently labeled plasma, the two outermost half-maximum points are used. Linear interpolation is used to add subpixel accuracy to the diameter measurement.

We now consider combining the velocity and diameter measurements to calculate flux. In laminar flow, the velocity $v(r)$ of the fluid through the pipe with radius R measured at a distance r from the center has a quadratic profile, with a maximal velocity $v(0)$ in the center and tapering to 0

Cite this article as *Cold Spring Harb Protoc*; 2013; doi:10.1101/pdb.prot076513

at the edges, that is

$$v(r) = v(0)\left(1 - \frac{r^2}{R^2}\right). \quad (1)$$

Measurements of RBC velocity as a function of distance from the vessel center show that this model is a close approximation (Schaffer et al. 2006), although systematic deviations result from the non-negligible size of the red blood cells. This tends to flatten the profile, and prevents the velocity from reaching 0 at the edges of the vessel. Neglecting these effects, the integrated flux through the vessel is given by (Helmchen and Kleinfeld 2008)

$$F = (1/2)v(0)\pi R^2. \quad (2)$$

In our example, both vessel diameter and RBC velocity in the arteriole respond to somatotopic stimulation. The flux through the arteriole increases by ~100% over baseline, compared with 35% and 40% for diameter and velocity measurements alone, respectively (Fig. 2F). Because the scan path runs at 733 Hz in this example, the diameter and RBC velocity traces are collected nearly simultaneously from both the penetrating arteriole and ascending venule.

Generation of Spatially Optimized Line Scans

The microscope laser is directed by a pair of fast *x*–*y* scan mirrors (Cambridge Technology, 6210H galvometer optical scanner with MicroMax 673xx dual-axis servo driver). The mirror controller uses a closed loop position feedback system to accurately map control voltage to mirror position. The position accurately tracks the control voltage, with ~90 μsec delay.

To create an arbitrary scanning path, several full-frame images of the region containing the desired vessels are first acquired and averaged together to increase the signal-to-noise ratio. This image is loaded by custom software written in MATLAB (MathWorks), which allows users to interactively create lines of interest (i.e., scans across or along vessels) on the full frame image.

The mirror voltages used to acquire the original full frame image are known, so that positions on the image can be mapped one-to-one to mirror voltages. Linear portions of the scan path, such as those used to track along a vessel to measure RBC speed and those that span the vessel to measure diameter, are given by

$$P = P_0 + V_{\text{linear}}t, \quad (3)$$

where P and V are two-dimensional vectors that contain x and y coordinates.

Linear portions of the scan path, scanned at constant velocity, must be connected by a function that creates a physically realistic path for the mirrors to follow (Lillis et al. 2008). Although there are an arbitrary number of such functions, the simplest is a third-order polynomial given by

$$P_{\text{spline}} = P_i + V_i t + Ct^2 + Dt^3. \quad (4)$$

For computational convenience, the connecting spline is taken to start at $t = 0$, and end at $t = \tau$. The initial position P_i and velocity V_i of the spline are set to match the position and velocity of the end of the linear region preceding the spline.

The additional spline parameters depend on the length (in time) of the spline, τ, and the final position and velocity of the spline, and are given by

$$C = \frac{3P_f}{\tau^2} - \frac{3P_i}{\tau^2} - \frac{2V_i}{\tau} - \frac{V_f}{\tau} \quad (5)$$

and

$$D = \frac{V_f}{3\tau^2} - \frac{V_i}{3\tau^2} - \frac{2C}{3\tau}. \tag{6}$$

The value of τ used should be the smallest positive real value that does not subject the mirrors to an acceleration larger than a user-defined maximal value, m, typically 100 V/msec^2. Because the acceleration of the spline is a linear function of time, the extreme values of acceleration occur at the beginning and the end of the spline.

Candidate values for the shortest possible spline length are found by setting the mirror acceleration to $\pm m$ at the beginning and end of spline, and finding all positive real values for τ:

$$0 = \pm m\tau^2 + (2V_{i,x} + 4V_{f,x})\tau + (6P_{i,x} - 6P_{f,x}), \tag{7}$$

$$0 = \pm m\tau^2 + (2V_{i,y} + 4V_{f,y})\tau + (6P_{i,y} - 6P_{f,y}), \tag{8}$$

$$0 = \pm m\tau^2 + (4V_{i,x} + 2V_{f,x})\tau + (6P_{i,x} - 6P_{f,x}), \tag{9}$$

$$0 = \pm m\tau^2 + (4V_{i,y} + 2V_{f,y})\tau + (6P_{i,y} - 6P_{f,y}). \tag{10}$$

The actual time used is the smallest value that keeps the acceleration within limits at the beginning and end of the spline; that is, all of $|2C_x| < m$, $|2C_y| < m$, $|2C_x + 6D_x\tau| < m$, and $|2C_y + 6D_x\tau| < m$ are true.

Summary

Two-photon laser scanning microscopy offers a means to obtain high-resolution images of RBC velocity and vessel diameter in vivo. These measurements can be combined to calculate the flux for a given vessel, which is a more accurate metric of the oxygen- and nutrient-carrying capability of blood.

Velocity and diameter measurements can change independently (Fig. 2F) and thus they must be measured nearly simultaneously to accurately access flux. This can be achieved with the spatially optimized line-scan algorithm described above. This technique can be extended to image other types of fluorescent signals, for instance, neural activity as indicated by calcium-sensitive dyes. In principle, this technique can be readily extended to scan in three dimensions as well. However, the speed of current mechanical z-axis scanners is currently much slower than what can be achieved when scanning in the x–y plane alone (Göbel and Helmchen 2007; Göbel et al. 2007).

RECIPE

Modified Artificial Cerebrospinal Fluid (mACSF)

Reagent	Final concentration
NaCl	125 mM
Glucose	10 mM
HEPES	10 mM
$CaCl_2$	3.1 mM
$MgCl_2$	1.3 mM

Adjust the pH to 7.4. This mACSF is free of carbonate and phosphate. The recipe is taken from Kleinfeld and Delaney (1996).

ACKNOWLEDGMENTS

We thank Quoc-Thang Nguyen for useful discussions on MPScope scan software. This work was funded by the National Institutes of Health (grants EB003832, NS059832, and RR021907 to D.K. and AG029681 to G.C.), the National Science Foundation (grant DBI 0455027), and a postdoctoral fellowship from the American Heart Association to A.Y.S.

REFERENCES

Devor A, Tian P, Nishimura N, Teng IC, Hillman EM, Narayanan SN, Ulbert I, Boas DA, Kleinfeld D, Dale AM. 2007. Suppressed neuronal activity and concurrent arteriolar vasoconstriction may explain negative blood oxygenation level-dependent signaling. *J Neurosci* **27:** 4452–4459.

Drew PJ, Feldman DE. 2009. Intrinsic signal imaging of deprivation-induced contraction of whisker representations in rat somatosensory cortex. *Cereb Cortex* **19:** 331–348.

Drew PJ, Blinder P, Cauwenberghs G, Shih AY, Kleinfeld D. 2010a. Rapid determination of particle velocity from space-time images using the Radon transform. *J Comput Neurosci* **29:** 5–11.

Drew PJ, Shih AY, Driscoll JD, Knutsen PM, Blinder P, Davalos D, Akassoglou K, Tsai PS, Kleinfeld D. 2010b. Chronic optical access through a polished and reinforced thinned skull. *Nat Meth* **7:** 981–984.

Göbel W, Helmchen F. 2007. New angles on neuronal dendrites in vivo. *J Neurophysiol* **98:** 377–379.

Göbel W, Kampa BM, Helmchen F. 2007. Imaging cellular network dynamics in three dimensions using fast 3D laser scanning. *Nat Meth* **4:** 73–79.

Helmchen F, Kleinfeld D. 2008. In vivo measurements of blood flow and glial cell function with two photon laser scanning microscopy. *Methods Enzymol* **444:** 231–254.

Kleinfeld D, Delaney KR. 1996. Distributed representation of vibrissa movement in the upper layers of somatosensory cortex revealed with voltage sensitive dyes. *J Comp Neurol* **375:** 89–108.

Kleinfeld D, Denk W. 2000. Two-photon imaging of neocortical microcirculation. In *Imaging neurons: A laboratory manual* (ed. Yuste R, et al.), pp. 23.1–23.15. Cold Spring Harbor Laboratory Press, Cold Spring Harbor, NY.

Kleinfeld D, Mitra PP, Helmchen F, Denk W. 1998. Fluctuations and stimulus-induced changes in blood flow observed in individual capillaries in layers 2 through 4 of rat neocortex. *Proc Natl Acad Sci* **95:** 15741–15746.

Lillis KP, Eng A, White JA, Mertz J. 2008. Two-photon imaging of spatially extended neuronal network dynamics with high temporal resolution. *J Neurosci Methods* **172:** 178–184.

Mostany R, Portera-Cailliau C. 2008. A craniotomy surgery procedure for chronic brain imaging. *J Vis Exp* **4:** 1128–1144.

Nguyen Q-T, Tsai PS, Kleinfeld D. 2006. MPScope: A versatile software suite for multiphoton microscopy. *J Neurosci Methods* **156:** 351–359.

Nguyen Q-T, Dolnick EM, Driscoll J, Kleinfeld D. 2009. MPScope 2.0: A computer system for two-photon laser scanning microscopy with concurrent plasma-mediated ablation and electrophysiology. In *Methods for in vivo optical imaging*, 2nd ed. (ed. Frostig RD.), pp. 117–142. CRC Press, Boca Raton, FL.

Paxinos G, Watson C. 1986. *The rat brain in stereotaxic coordinates.* Academic, San Diego.

Schaffer CB, Friedman B, Nishimura N, Schroeder LF, Tsai PS, Ebner FF, Lyden PD, Kleinfeld D. 2006. Two-photon imaging of cortical surface microvessels reveals a robust redistribution in blood flow after vascular occlusion. *Pub Libr Sci Biol* **4:** 258–270.

Tsai PS, Kleinfeld D. 2009. In vivo two-photon laser scanning microscopy with concurrent plasma-mediated ablation: Principles and hardware realization. In *Methods for in vivo optical imaging*, 2nd ed. (ed. Frostig RD.), pp. 59–115. CRC Press, Boca Raton, FL.